Received 18 July 2022; revised 5 October 2022; accepted 10 October 2022. Date of publication 12 October 2022; date of current version 21 October 2022.
The review of this article was arranged by Editor M. K. Radhakrishnan.

Digital Object Identifier 10.1109/JEDS.2022.3214000

Low Interface Trapped Charge Density for Al_2O_3/β-Ga_2O_3 (001) Metal-Insulator-Semiconductor Capacitor

QIHAO ZHANG [1], YISONG SHEN [1], JIANGWEI LIU [2], CHUNMING TU [1] (Senior Member, IEEE), DONGYUAN ZHAI [1], MIN HE [1], AND JIWU LU [1] (Member, IEEE)

1 College of Electrical and Information Engineering, Hunan University, Changsha 410082, Hunan, China

2 Research Center for Functional Materials, National Institute for Materials Science, Ibaraki 305-0044, Japan

CORRESPONDING AUTHOR: J. LU (e-mail: jiwu_lu@hnu.edu.cn)

This work was supported in part by the National Key Research and Development Program of China under Grant 2018YFB1201802; in part by the National Natural Science Foundation of China under Grant 51977065 and Grant 52177179; and in part by the Science and Technology Innovation Program of Hunan Province, People's Republic of China, under Grant 2019RS1024 and Grant 2020RC5004.

ABSTRACT In this letter, high-performance Al_2O_3/β-Ga_2O_3 (001) metal-insulator-semiconductor (MIS) capacitor has been demonstrated. The capacitance-voltage (C–V) curves of the Al_2O_3/β-Ga_2O_3 (001) MIS capacitor remain stable under different measurement frequencies. The leakage current density is lower than 2.0×10^{-8} A/cm^2 when the gate voltage is in the range of $-5\sim13$ V. The fixed charge and trapped charge densities in Al_2O_3 film are 4.4×10^{12} and 6.0×10^{11} cm^{-2}, respectively. Average and minimum interface trapped charge density (D_{it}) for Al_2O_3/β-Ga_2O_3 (001) interface has been extracted to be as low as 3.3×10^{11} and 2.3×10^{11} cm^{-2} eV^{-1} via the Terman method, respectively. The low D_{it} is probably attributed to the modification of vacancy defects and the introduction of hydroxyl groups at the Al_2O_3/β-Ga_2O_3 (001) interface after piranha solution pretreatment for β-Ga_2O_3.

INDEX TERMS β-Ga_2O_3, Al_2O_3, MIS capacitor, interface trapped charge density.

I. INTRODUCTION

Over the last couple of years, wide bandgap semiconductor materials such as SiC, GaN, and Ga_2O_3 have attracted lots of attention for power device applications due to their outstanding material properties [1], [2], [3]. Among them, Ga_2O_3 with an ultra-wide bandgap of 4.6-4.9 eV, high critical breakdown field of 8 MV/cm, and high Baliga's Figure-of-Merit of 3214 has been considered as a more desirable semiconductor material for the next-generation power devices [3]. Furthermore, wide-range controllable *n*-type doping (10^{16}-10^{19} cm^{-3}) and mass production large size β-Ga_2O_3 single crystal wafers have been commercially available [3]. Due to these superiorities, β-Ga_2O_3 has been applied to power Schottky diodes, metal-semiconductor field-effect transistors (FETs) and metal-insulator-semiconductor FETs (MISFETs) [3], [4], [5], [6], [7], [8], [9].

Recently, the planar and vertical β-Ga_2O_3-based MISFETs with high breakdown voltages and low on-resistance have been demonstrated [5], [6], [7], [8], [9]. The high-quality dielectric/β-Ga_2O_3 heterostructure is significantly important for fabricating high-performance MISFETs. Among all the dielectric materials, Al_2O_3 is used most widely in CMOS devices owing to its high dielectric constant, high thermal stability, and high breakdown electric field [10], [11], [12]. Additionally, it has a large conduction band offset (ΔE_C) with β-Ga_2O_3 [13], [14]. Continuous efforts focusing on investigating the interface trapped charge density (D_{it}) for Al_2O_3/β-Ga_2O_3 MIS capacitors have been reported. Due to the significant asymmetry of monoclinic β-Ga_2O_3 [3], [4], the D_{it} values are apparently different for the Al_2O_3 on the various planes of β-Ga_2O_3.

Hirose et al. improved the D_{it} for the Al_2O_3/β-Ga_2O_3 (001) to be $\sim1.6 \times 10^{12}$ cm^{-2} eV^{-1} by the low-temperature post-deposition annealing (PDA) process [15]. In consideration of the effect for bulk traps, Jian et al. clarified the D_{it} of 1.3×10^{12} cm^{-2} eV^{-1} for Al_2O_3/β-Ga_2O_3

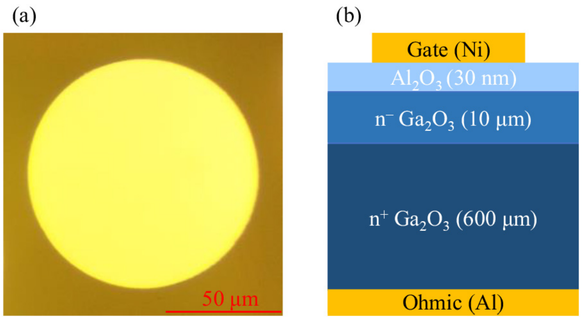

FIGURE 1. **(a) Surface morphology and (b) cross-sectional schematic diagram of the Al_2O_3/β-Ga_2O_3 (001) MIS capacitor, respectively.**

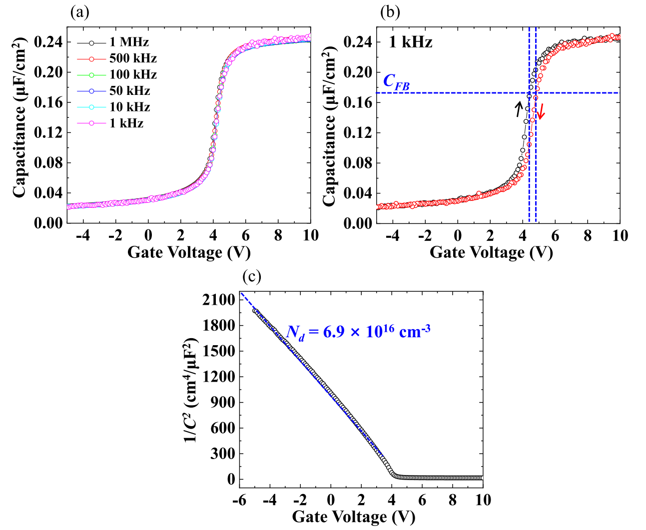

FIGURE 2. **(a) Frequency dependent *C–V* characteristics, (b) hysteresis *C–V* curves at 1 kHz, and (c) $1/C^2$ as a function of gate voltage for the Al_2O_3/β-Ga_2O_3 (001) MIS capacitor, respectively.**

(001) using the deep ultraviolet (DUV)-assisted method [16]. Feng et al. adopted a novel Ga flux etching surface treatment to decrease the D_{it} of Al_2O_3/β-Ga_2O_3 (001) to be 7.3 $\times$ 10^{11} cm^{-2} eV^{-1} [17]. By an in-situ deposition technique for the Al_2O_3, Roy et al. obtained a low D_{it} of 6.4 $\times$ 10^{11} cm^{-2} eV^{-1} for the Al_2O_3/β-Ga_2O_3 (001) MIS capacitor [18]. Jayawardena et al. clarified the effects of different gate dielectrics (SiO_2 and Al_2O_3) on the D_{it} of the β-Ga_2O_3 (−201) MIS capacitors and concluded that the Al_2O_3/β-Ga_2O_3 (−201) interface had a lower D_{it} of 8.4 $\times$ 10^{11} cm^{-2} eV^{-1} [19]. By combining piranha solution pretreatment and the PDA process, Zhou et al. obtained the D_{it} for Al_2O_3/β-Ga_2O_3 (−201) as low as 2.3 $\times$ 10^{11} cm^{-2} eV^{-1} [20].

The Al_2O_3 on the β-Ga_2O_3 (001) exhibited higher D_{it} near conduction band (E_C) than those on β-Ga_2O_3 (−201) and (010). This is undesirable to enable high-performance β-Ga_2O_3 (001)-based MISFETs. This work focuses on decreasing the D_{it} for the Al_2O_3/β-Ga_2O_3 (001) with the piranha solution pretreatment for the β-Ga_2O_3. The frequency-dependent current-voltage (*C–V*) property, gate leakage current density (*J*), and band configuration for Al_2O_3/β-Ga_2O_3 (001) will also be investigated and discussed.

II. EXPERIMENTAL DETAILS

The MIS capacitors were fabricated on an *n*-type β-Ga_2O_3 (001) substrate with a 10 μm lightly Si-doped epitaxial layer. The bulk substrate and epitaxial layer were grown by edge-defined film-fed growth and hydride vapor phase epitaxy technologies, respectively. Their doping concentrations were around 5 $\times$ 10^{18} cm^{-3} and 7 $\times$ 10^{16} cm^{-3}, respectively. After cleaning the β-Ga_2O_3 epitaxial wafer in acetone for 3 min and alcohol for 3 min, the sample was treated in piranha solution for 5 min. The piranha solution volume ratio for the H_2O_2, H_2SO_4, and deionized water was 1: 4: 1. A 30 nm-thick Al_2O_3 film was deposited as the gate dielectric on the β-Ga_2O_3 (001) epitaxial layer via an atomic layer deposition (ALD) system. The precursors were tri-methyl-aluminum (TMA) and water vapor. The ALD deposition temperature and chamber pressure were 300 °C and 60 Pa, respectively. The aluminum (Al) metal was thermally evaporated on the backside of the substrate to form Ohmic contact. Gate contact of nickel (Ni) was evaporated on the top of the Al_2O_3 film to finish the fabrication process. The frequency-dependent *C–V* and *J–V* characterizations of the MIS capacitor were carried out via an Agilent B1500A semiconductor device analyzer.

III. RESULTS AND DISCUSSION

Fig. 1(a) and 1(b) show the surface morphology and cross-sectional schematic diagram of the β-Ga_2O_3 MIS capacitor, respectively. The circular radius and area of the gate electrode are 50 μm and 7.85 $\times$ 10^{-5} cm^{-2}, respectively.

Fig. 2(a) shows the frequency-dependent *C-V* curves of the Al_2O_3/β-Ga_2O_3 (001) MIS capacitor. The gate voltage sweeps from −5 V to 10 V and the frequency varies from 1 kHz to 1 MHz. The measurement capacitance values remain stable with the variation of measurement frequency. An insignificant frequency dispersion phenomenon is observed. The oxide capacitance (C_{OX}) of the Al_2O_3/β-Ga_2O_3 (001) MIS capacitor is determined to be 0.24 $\mu F/cm^2$. By considering the thickness of Al_2O_3 (30 nm), the dielectric constant of the Al_2O_3 is calculated to be 8.1, which is in agreement with the previous reports [21], [22].

Fig. 2(b) shows the hysteresis characteristic of *C–V* curves for the Al_2O_3/β-Ga_2O_3 (001) MIS capacitor at 1 kHz. The measurement voltages change from −5 V to 10 V (black line) and then sweep in the opposite direction (red line). The flat band voltage (V_{FB}) is determined to be 4.4 V according to the position of flat-band capacitance (C_{FB}) [23]. The large positive shift of V_{FB} is ascribed to the presence of negative fixed charges in the Al_2O_3 film, which is confirmed in the previous report [19]. The change of the ALD-Al_2O_3 precursor with ozone or PDA process may alleviate the shift of V_{FB} [20].

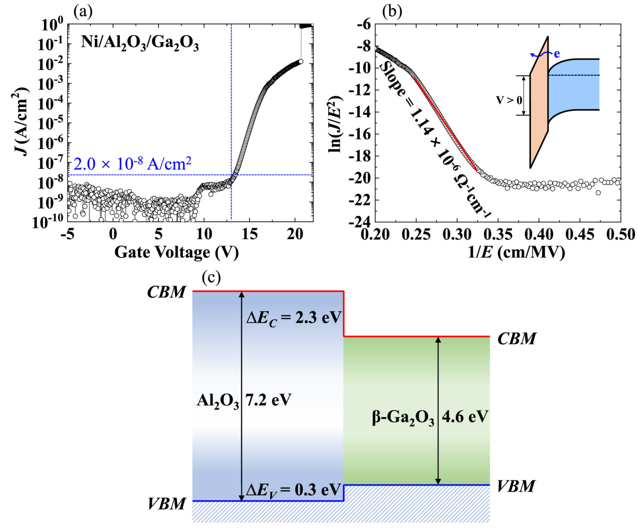

FIGURE 3. **(a) The *J–V* characteristic, (b) ln(J/E^2) vs 1/*E* for Al_2O_3/β-Ga_2O_3 MIS capacitor, and (c) the energy band diagram for Al_2O_3/β-Ga_2O_3 heterojunction, respectively.**

The negative fixed charges density (Q_f) is computed to be 4.4×10^{12} cm^{-2} by the following equation (1):

$$Q_f = C_{OX} \times \left(V_{FB} - \frac{\Phi_{MS}}{q}\right), \quad (1)$$

where Φ_{MS} denotes the difference in work functions between Ni (5.15 eV) and β-Ga_2O_3 (3.71 eV) [24], [25]. A typical *C–V* hysteresis phenomenon exists in the *C–V* curves of the Al_2O_3/β-Ga_2O_3 (001) MIS capacitor. The hysteresis voltage is extracted to be 0.4 V, indicating the presence of trapped charge or border traps in the Al_2O_3 film. The trapped charge density is computed to be 6.0×10^{11} cm^{-2}, which is competitive with the previous reports [17], [18], [19]. The $1/C^2$ as a function of gate voltage is shown in Fig. 2(c). The donor concentration (N_d) of the Al_2O_3/β-Ga_2O_3 (001) is extracted to be 6.9×10^{16} cm^{-3}.

The *J–V* characteristic of the Al_2O_3/β-Ga_2O_3 (001) MIS capacitor is shown in Fig. 3(a). The *J* values are lower than 2×10^{-8} A/cm^{-2} when the gate voltage sweeps from −5 V to 13 V. This indicates that the high-quality Al_2O_3 film and good Al_2O_3/β-Ga_2O_3 (001) interface are formed. When the gate voltage reaches 20 V, there is an obvious hard breakdown phenomenon for the Ni/Al_2O_3/β-Ga_2O_3 MIS capacitor. To further investigate the leakage current mechanism of the Al_2O_3/β-Ga_2O_3 (001) MIS capacitor, the Fowler–Nordheim (FN) tunneling model was taken into account after excluding other models such as Poole–Frenkel model, trap-assisted tunneling, Schottky emission [26], [27], [28], [29]. Fig. 3(b) shows the ln(J/E^2) versus *1/E* curve of the β-Ga_2O_3 MIS capacitor. The linear relationship is observed under high electrical fields (*1/E* < 0.33 cm/MV), which is in agreement with the FN tunneling model based on the following equation (2):

$$J = \frac{q^3 m_{sc} E^2}{8\pi h m^* \Phi_B} E^2 exp\left(-\frac{8\pi\sqrt{2m^*\Phi_B{}^3}}{3hq}\frac{1}{E}\right), \quad (2)$$

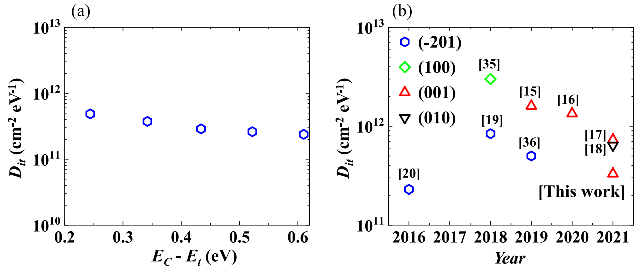

FIGURE 4. **(a) The extracted D_{it} vs E_c-E_t determined by Terman method for the Al_2O_3/β-Ga_2O_3 (001) interface. (b) Benchmarking plot of D_{it} values for Al_2O_3 on β-Ga_2O_3 with different planes.**

where m^* is the effective electron mass in Al_2O_3 film (0.23 m_0, m_0 is the electron effective mass) [30], m_{sc} is the effective electron mass in β-Ga_2O_3, Φ_B is the tunneling barrier height for electrons or the ΔE_C for the Al_2O_3/β-Ga_2O_3 (001) heterojunction, *h* is the Planck's constant, *E* denotes the electrical field across the gate oxide, and *q* is the electron charge, respectively. By fitting linear regions of ln(J/E^2)−*1/E* characteristic, the slope is extracted to be 1.14×10^{-6} $\Omega^{-1}cm^{-1}$. Therefore, the Φ_B is determined to be 2.3 eV for the Al_2O_3/β-Ga_2O_3 (001) heterojunction based on equation (2). It agrees with the previously reported value deduced via an X-ray photoelectron spectroscopy technique [31]. The large ΔE_C for the Al_2O_3/β-Ga_2O_3 (001) could explain the low *J* for the MIS capacitor. The energy band diagram of the Al_2O_3/β-Ga_2O_3 (001) heterostructure is shown in Fig. 3(c). The *VBM*, *CBM*, and E_g are valence band maximum, conduction band minimum, and bandgap energy, respectively. The valence band offset (ΔE_V) is determined to be 0.3 eV in consideration of the E_g for Al_2O_3 (7.2 eV) and β-Ga_2O_3 (4.6 eV) [32], [33]. Band configuration for the Al_2O_3/β-Ga_2O_3 (001) heterojunction exhibits a type I (straddling gap) structure.

The D_{it} can be extracted via the Terman method, which is recognized to evaluate accurately D_{it} information of over 10^{10} cm^{-2} eV^{-1} [34]. The gate voltage of the ideal high-frequency *C–V* curve obtained by the numerical method is compared with that of the actual curve to achieve the D_{it} values via the following equation (3):

$$D_{it} = \frac{C_{OX}}{q^2}\left(\frac{dV}{d\varphi_s} - 1\right) - \frac{C_s}{q} = \frac{C_{OX}}{q^2}\frac{d\Delta V}{d\varphi_s}, \quad (3)$$

where the φ_s is the surface potential of the β-Ga_2O_3 (001), ΔV is the difference between real gate voltage and ideal ones, and C_s is semiconductor capacitance. Because of the limitations of direct current sweep rate and alternating current frequency, the D_{it} is detected in the trap energy level (E_t) range of E_C-0.2 < E_t < E_C-0.6 eV. Fig. 4 (a) shows the extracted D_{it} distribution versus E_C-E_t. With the increase of E_C-E_t, the D_{it} decreases. The average and minimum D_{it} values are 3.3×10^{11} and 2.3×10^{11} cm^{-2} eV^{-1}, respectively.

Fig. 4 (b) summarizes previously reported D_{it} values for Al_2O_3 on the different planes of β-Ga_2O_3. The average D_{it} in this work is much lower than those of the Al_2O_3 on β-Ga_2O_3 (001), (010), and (100) of the previous reports [15], [16], [17], [18], [35]. It is also comparable with the minimum value of the Al_2O_3/β-Ga_2O_3 (−201) [19], [20], [36]. This indicates that the high-quality Al_2O_3/β-Ga_2O_3 (001) interface has been formed by the piranha solution for the β-Ga_2O_3 (001). The low D_{it} for the Al_2O_3/β-Ga_2O_3 (001) is possibly attributed to the following two factors. The vacancy (e.g., oxygen vacancies) defects, expected to act as the trapped charge at the Al_2O_3/β-Ga_2O_3 interface, may be modified after the piranha pretreatment [37], [38]. On the other hand, the piranha pretreatment probably introduces hydroxyl groups on the surface of β-Ga_2O_3, which could promote the chemical reaction of TMA with water vapor during the first growth stage of the ALD-Al_2O_3 film [39], [40]. This could increase the quality of the Al_2O_3/β-Ga_2O_3 (001) interface and make the D_{it} decrease.

IV. CONCLUSION

In this study, we have fabricated the Al_2O_3/β-Ga_2O_3 (001) MIS capacitor with the low D_{it}. The absence of frequency dispersion for the β-Ga_2O_3 MIS capacitor was observed from frequency-dependent C–V curves. The positive C–V curves shift indicates the existence of the negative fixed charges in the Al_2O_3 film. The Al_2O_3/β-Ga_2O_3 heterojunction shows a high ΔE_C of 2.3 eV based on the FN tunneling model. The average D_{it} near E_C was extracted to be as low as 3.3×10^{11} cm^{-2} eV^{-1} by the Terman method. The low D_{it} may be ascribed to the modification of vacancy defects and the promotion of chemical reaction of TMA with water vapor due to the introduction of hydroxyl groups after the piranha pretreatment.

REFERENCES

[1] X. She, A. Q. Huang, O. Lucia, and B. Ozpineci, "Review of silicon carbide power devices and their applications," *IEEE Trans. Ind. Electron.*, vol. 64, no. 10, pp. 8193–8205, Oct. 2017, doi: 10.1109/TIE.2017.2652401.

[2] E. A. Jones, F. F. Wang, and D. Costinett, "Review of commercial GaN power devices and GaN-based converter design challenges," *IEEE J. Emerg. Sel. Topics Power Electron.*, vol. 4, no. 3, pp. 707–719, Sep. 2016, doi: 10.1109/JESTPE.2016.2582685.

[3] S. J. Pearton et al., "A review of Ga_2O_3 materials, processing, and devices," *Appl. Phys. Rev.*, vol. 5, no. 1, Mar. 2018, Art. no. 11301, doi: 10.1063/1.5006941.

[4] S. J. Pearton, F. Ren, M. Tadjer, and J. Kim, "Perspective: Ga_2O_3 for ultra-high power rectifiers and MOSFETs," *J. Appl. Phys.*, vol. 124, no. 22, 2018, Art. no. 220901, doi: 10.1063/1.5062841.

[5] W. Li, K. Nomoto, Z. Hu, T. Nakamura, D. Jena, and H. G. Xing, "Single and multi-fin normally-off Ga_2O_3 vertical transistors with a breakdown voltage over 2.6 kV," in *Proc. IEEE Int. Electron Devices Meeting (IEDM)*, San Francisco, CA, USA, Dec. 2019, p. 12, doi: 10.1109/IEDM19573.2019.8993526.

[6] Z. A. Jian, S. Mohanty, and E. Ahmadi, "Switching performance analysis of 3.5 kV Ga_2O_3 power FinFETs," *IEEE Trans. Electron Devices*, vol. 68, no. 2, pp. 672–678, Feb. 2021, doi: 10.1109/TED.2020.3043988.

[7] Y. Wang et al., "Demonstration of β-Ga2O3 superjunction-equivalent MOSFETs," *IEEE Trans. Electron Devices*, vol. 69, no. 4, pp. 2203–2209, Apr. 2022, doi: 10.1109/TED.2022.3152464.

[8] K. Tetzner et al., "Lateral 1.8 kV β-Ga_2O_3 MOSFET with 155 MW/cm^2 power figure of merit," *IEEE Electron Device Lett.*, vol. 40, no. 9, pp. 1503–1506, Sep. 2019, doi: 10.1109/LED.2019.2930189.

[9] Y. Lv et al., "Source-field-plated β-Ga_2O_3 MOSFET with record power figure of merit of 50.4 MW/cm^2," *IEEE Electron Device Lett.*, vol. 40, no. 1, pp. 83–86, Jan. 2019, doi: 10.1109/LED.2018.2881274.

[10] G. He, X. Chen, and Z. Sun, "Interface engineering and chemistry of Hf-based high-k dielectrics on III–V substrates," *Surface Sci. Rep.*, vol. 68, no. 1, pp. 68–107, Mar. 2013, doi: 10.1016/j.surfrep.2013.01.002.

[11] G. He, J. Gao, H. Chen, J. Cui, Z. Sun, and X. Chen, "Modulating the interface quality and electrical properties of HfTiO/InGaAs gate stack by atomic-layer-deposition-derived Al_2O_3 passivation layer," *ACS Appl. Mater. Interfaces*, vol. 6, no. 24, pp. 22013–22025, Dec. 2014, doi: 10.1021/am506351u.

[12] G. Juan et al., "Passivation of Ge surface treated with trimethylaluminum and investigation of electrical properties of HfTiO/Ge gate stacks," *J. Mater. Sci. Technol.*, vol. 33, no. 8, pp. 901–906, Aug. 2017, doi: 10.1016/j.jmst.2017.04.021.

[13] T. Kamimura et al., "Band alignment and electrical properties of Al_2O_3/β-Ga_2O_3 heterojunctions," *Appl. Phys. Lett.*, vol. 104, no. 19, May 2014, Art. no. 192104, doi: 10.1063/1.4876920.

[14] T.-H. Hung et al., "Energy band line-up of atomic layer deposited Al_2O_3 on β-Ga_2O_3," *Appl. Phys. Lett.*, vol. 104, no. 16, Apr. 2014, Art. no. 162106, doi: 10.1063/1.4873546.

[15] M. Hirose et al., "Influence of post-deposition annealing on characteristics of Pt/Al_2O_3/β-Ga_2O_3 MOS capacitors," *Microelectron. Eng.*, vol. 216, Aug. 2019, Art. no. 111040, doi: 10.1016/j.mee.2019.111040.

[16] Z. Jian, S. Mohanty, and E. Ahmadi, "Deep UV-assisted capacitance–voltage characterization of post-deposition annealed Al_2O_3/β-Ga_2O_3 (001) MOSCAPs," *Appl. Phys. Lett.*, vol. 116, no. 24, Jun. 2020, Art. no. 242105, doi: 10.1063/5.0011144.

[17] B. Feng et al., "Reduction of MOS interfacial states between β-Ga_2O_3 and Al_2O_3 insulator by self-reaction etching with Ga flux," *Appl. Phys. Lett.*, vol. 118, no. 18, May 2021, Art. no. 181602, doi: 10.1063/5.0048311.

[18] S. Roy et al., "In situ dielectric Al_2O_3/β-Ga_2O_3 interfaces grown using metal–Organic chemical vapor deposition," *Adv. Electron. Mater.*, vol. 7, no. 11, Nov. 2021, Art. no. 2100333, doi: 10.1002/aelm.202100333.

[19] A. Jayawardena, R. P. Ramamurthy, A. C. Ahyi, D. Morisette, and S. Dhar, "Interface trapping in (−201) β-Ga_2O_3 MOS capacitors with deposited dielectrics," *Appl. Phys. Lett.*, vol. 112, no. 19, May 2018, Art. no. 192108, doi: 10.1063/1.5019270.

[20] H. Zhou, S. Alghamdi, M. Si, G. Qiu, and P. D. Ye, "Al_2O_3/β-Ga_2O_3 (−201) interface improvement through piranha pretreatment and post-deposition annealing," *IEEE Electron Device Lett.*, vol. 37, no. 11, pp. 1411–1414, Nov. 2016, doi: 10.1109/led.2016.2609202.

[21] M. D. Groner, J. W. Elam, F. H. Fabreguette, and S. M. George, "Electrical characterization of thin Al_2O_3 films grown by atomic layer deposition on silicon and various metal substrates," *Thin Solid Films*, vol. 413, nos. 1–2, pp. 186–197, Jun. 2002, doi: 10.1016/S0040-6090(02)00438-8.

[22] F. Argall and A. K. Jonscher, "Dielectric properties of thin films of aluminium oxide and silicon oxide," *Thin Solid Films*, vol. 2, no. 3, pp. 185–210, Sep. 1968, doi: 10.1016/0040-6090(68)90002-3.

[23] E. H. Nicollian and J. R. Brews, *MOS (Metal Oxide Semiconductor) Physics and Technology*. New York, NY, USA: Wiley, 1982.

[24] S. Gowtham, M. Deshpande, A. Costales, and R. Pandey, "Structural, energetic, electronic, bonding, and vibrational properties of Ga_3O, Ga_3O_2, Ga_3O_3, Ga_2O_3, and GaO_3 clusters," *J. Phys. Chem. B*, vol. 109, no. 31, pp. 14836–14844, Aug. 2005, doi: 10.1021/jp050801u.

[25] J. D. Guo, F. M. Pan, M. S. Feng, R. J. Guo, P. F. Chou, and C. Y. Chang, "Schottky contact and the thermal stability of Ni on n-type GaN," *J. Appl. Phys.*, vol. 80, no. 3, pp. 1623–1627, Aug. 1996, doi: 10.1063/1.363822.

[26] J. R. Yeargan and H. L. Taylor, "The Poole-frenkel effect with compensation present," *J. Appl. Phys.*, vol. 39, no. 12, pp. 5600–5604, Nov. 1968, doi: 10.1063/1.1656022.

[27] S. Fleischer, P. T. Lai, and Y. C. Cheng, "A new method for extracting the trap energy in insulators," *J. Appl. Phys.*, vol. 73, no. 7, pp. 3348–3351, Apr. 1993, doi: 10.1063/1.352934.

[28] P. W. Peacock and J. Robertson, "Band offsets and Schottky barrier heights of high dielectric constant oxides," *J. Appl. Phys.*, vol. 92, no. 8, pp. 4712–4721, Oct. 2002, doi: 10.1063/1.1506388.

[29] M. Lenzlinger and E. H. Snow, "Fowler-nordheim tunneling into thermally grown SiO_2," *J. Appl. Phys.*, vol. 40, no. 1, pp. 278–283, Jan. 1969, doi: 10.1063/1.1657043.

[30] J. Lin, S. Monaghan, K. Cherkaoui, I. M. Povey, B. Sheehan, and P. K. Hurley, "Examining the relationship between capacitance-voltage hysteresis and accumulation frequency dispersion in InGaAs metal-oxide-semiconductor structures based on the response to post-metal annealing," *Microelectron. Eng.*, vol. 178, pp. 204–208, Jun. 2017, doi: 10.1016/j.mee.2017.05.020.

[31] P. H. Carey et al., "Band alignment of Al_2O_3 with (−201) β-Ga_2O_3," *Vacuum*, vol. 142, pp. 52–57, Aug. 2017, doi: 10.1016/j.vacuum.2017.05.006.

[32] J. W. Liu, M. Y. Liao, M. Imura, and Y. Koide, "Band offsets of Al_2O_3 and HfO_2 oxides deposited by atomic layer deposition technique on hydrogenated diamond," *Appl. Phys. Lett.*, vol. 101, no. 25, Dec. 2012, Art. no. 252108, doi: 10.1063/1.4772985.

[33] P. H. Carey et al., "Band offsets in ITO/Ga_2O_3 heterostructures," *Appl. Surface Sci.*, vol. 422, pp. 179–183, Nov. 2017, doi: 10.1016/j.apsusc.2017.05.262.

[34] D. K. Schroder, *Semiconductor Material and Device Characterization*. Hoboken, NJ, USA: Wiley, 2006, pp. 342–364.

[35] H. Dong et al., "C-V and J-V investigation of HfO_2/Al_2O_3 bilayer dielectrics MOSCAPs on (100) β-Ga_2O_3," *AIP Adv.*, vol. 8, no. 6, Jun. 2018, Art. no. 65215, doi: 10.1063/1.5031183.

[36] D. Biswas, C. Joishi, J. Biswas, K. Thakar, S. Rajan, and S. Lodha, "Enhanced n-type β-Ga_2O_3 (−201) gate stack performance using Al_2O_3/SiO_2 bi-layer dielectric," *Appl. Phys. Lett.*, vol. 114, no. 21, May 2019, Art. no. 212106, doi: 10.1063/1.5089627.

[37] X. Ma, Y. Zhang, L. Dong, and R. Jia, "First-principles calculations of electronic and optical properties of aluminum-doped β-Ga_2O_3 with intrinsic defects," *Results Phys.*, vol. 7, pp. 1582–1589, Jan. 2017, doi: 10.1016/j.rinp.2017.04.023.

[38] J. Park and S.-M. Hong, "First principles calculation of band offsets and defect energy levels in Al2O3/β-Ga2O3 interface structures with point defects," *J. Semicond. Technol. Sci.*, vol. 19, no. 4, pp. 413–425, Aug. 2019, doi: 10.5573/JSTS.2019.19.4.413.

[39] B. Huang, M. Zheng, Y. Zhao, J. Wu, and J. T. L. Thong, "Atomic layer deposition of high-quality Al_2O_3 thin films on MoS_2 with water plasma treatment," *ACS Appl. Mater. Interfaces*, vol. 11, no. 38, pp. 35438–35443, Sep. 2019, doi: 10.1021/acsami.9b10940.

[40] H. Wang, H. Zhang, J. Liu, D. Xue, H. Liang, and X. Xia, "Hydroxyl group adsorption on GaN (0001) surface: First principles and XPS studies," *J. Electron. Mater.*, vol. 48, no. 4, pp. 2430–2437, Apr. 2019, doi: 10.1007/s11664–019–07011–1.